Biomaterials 269 (2021) 120643

Contents lists available at ScienceDirect

Biomaterials

journal homepage: www.elsevier.com/locate/biomaterials

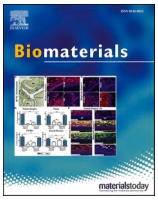

Rheological characterization, compression, and injection molding of hydroxyapatite-silk fibroin composites

Stephanie L. McNamara [a,c], Ethan M. McCarthy [b], Daniel F. Schmidt [b], Stephen P. Johnston [b], David L. Kaplan [a,*]

[a] Department of Biomedical Engineering, Tufts University, Medford, MA, USA
[b] Department of Plastics Engineering, University of Massachusetts Lowell, Lowell, MA, USA
[c] Harvard John A. Paulson School of Engineering and Applied Sciences, Harvard University, Cambridge, MA, USA

ARTICLE INFO

Keywords:
Silk-ceramic composites
Injection molding
Compression molding
Bone grafts
Orthopedic implants

ABSTRACT

Traditional bone fixation devices made from inert metal alloys provide structural strength for bone repair but are limited in their ability to actively promote bone healing. Although several naturally derived bioactive materials have been developed to promote ossification in bone defects, it is difficult to translate small-scale benchtop fabrication of these materials to high-output manufacturing. Standard industrial molding processes, such as injection and compression molding, have typically been limited to use with synthetic polymers since most biopolymers cannot withstand the harsh processing conditions involved in these techniques. Here we demonstrate injection and compression molding of a bioceramic composite comprised of hydroxyapatite (HA) and silk fibroin (SF) from *Bombyx mori* silkworm cocoons. Both the molding behavior of the HA-SF slurry and final scaffold mechanics can be controlled by modulating SF protein molecular weight, SF content, and powder-to-liquid ratio. HA-SF composites with up to 20 weight percent SF were successfully molded into stable three-dimensional structures using high pressure molding techniques. The unique durability of silk fibroin enables application of common molding techniques to fabricate composite silk-ceramic scaffolds. This work demonstrates the potential to move bone tissue engineering one step closer to large-scale manufacturing of natural protein-based resorbable bone grafts and fixation devices.

1. Introduction

Bone grafts and bone fixation devices should provide high structural stability and maintain functional alignment while simultaneously encouraging new bone formation [1–3]. Although metal alloys commonly used for bone repair meet the required strength criteria for load-bearing applications, they lack the ability to promote native bone healing. Synthetic polymers offer one alternative solution since they display tunable biosorption profiles allowing native bone replacement over time [4,5]. Since these materials, like most polymers, lack sufficient strength required for use as a bone replacement or fixation material, osteoinductive biopolymers have been combined with high strength bioceramics, such as hydroxyapatite, to create composite scaffolds [6–9]. These polymer composites, such as polylactic acid-hydroxyapatite, are readily formed using a variety of processing techniques ranging from 3D printing to injection molding [10–13]. However, unless combined with a delivered bioactive substance, synthetic polymers do not effectively stimulate cellular proliferation within the defect. Instead, natural biopolymers, such as collagen, fibrin, silk, and alginate, have been explored for use as bioactive implants due to their proven ability to induce bone remodeling [5,14–17].

Bioceramics are commonly used in bone tissue engineering due to their close similarity to the chemical structure of bone, their ability to integrate with native osseous tissue, and their capacity for slow resorption over time [18–20]. Composite implants comprised of polymeric and inorganic mineral phases leverage both the high compressive strength of ceramics as well as the high fracture toughness of polymers [21–23]. However, when it comes to manufacturing, ceramic composite molding is a complicated process that requires close attention to powder properties, packing density, binder selection, and flow characteristics, and involves a less standardized work flow than thermoplastic manufacturing due to added complications such as phase separation and

* Corresponding author. Tufts University, Department of Biomedical Engineering, 4 Colby Street, Medford, MA, 02155, USA.
E-mail addresses: Stm154@g.harvard.edu (S.L. McNamara), Ethan_McCarthy@student.uml.edu (E.M. McCarthy), Daniel_Schmidt@uml.edu (D.F. Schmidt), Stephen_Johnston@uml.edu (S.P. Johnston), David.Kaplan@tufts.edu (D.L. Kaplan).

https://doi.org/10.1016/j.biomaterials.2020.120643
Received 26 August 2020; Received in revised form 17 December 2020; Accepted 28 December 2020
Available online 2 January 2021

post-injection shrinkage [24–27]. Despite these challenges, ceramic injection molding can generate parts with higher complexity and tighter tolerances at a faster rate than standard ceramic manufacturing techniques, such as slip casting, uniaxial or cold isostatic pressing [28]. The durability of injection molds, typically made from steel, far exceeds the durability of the porous molds used for slip casting, typically made from plaster, thereby allowing for longer production runs and reduced variability. Unlike synthetic polymers, which exhibit thermoplastic behavior in that they readily flow when heated, most natural biopolymers will quickly aggregate or denature when exposed to the high pressure and high heat conditions used for industrial molding [29]. Proteins will fall out of solution during processing thereby impeding material flow into the molding cavity and resulting in an inhomogeneous product. Thus, there is a need for a mechanically robust yet bioactive natural polymer amenable to standard industrial processing in the orthopedic space.

The goal of this study was to investigate the feasibility of injection molding to fabricate composite scaffolds made of hydroxyapatite with regenerated silk fibroin from *Bombyx mori* silkworm cocoons. Silk fibroin is an ideal biopolymer for injection and compression molding due to its high stability and resistance to degradation in response to heat or shear stress. Silk can be processed into a variety of physical formats ranging from raw fiber to regenerated aqueous and organic solvent-based silk solutions that can be cast into various scaffold forms, and specific parameters of silk cocoon processing can be controlled to tune properties of the regenerated silk solution, such as molecular weight. These factors play a role in regulating the rheological behavior and flow of the regenerated silk solution as well as the structure of the final scaffold. Our previous work on silk consolidation casting of hydroxyapatite-silk composites has shown that silk can be used as an effective binder in the production of stable green bodies [30]. In combination with calcium phosphate ceramics, silk can increase the toughness of the mineral component providing a greater balance between strength and fracture resistance [31]. These advantages make silk fibroin well-suited for injection and compression molding to create composite scaffolds and implants. Although the use of silk fibroin in injectable calcium phosphate-based bone cements has been investigated previously [32,33], these studies have been mainly conducted using low, syringe-controlled injection speeds and pressures not comparable to the high flow rates and pressures associated with injection molding.

In this work we present how HA-SF composites were prepared, how the rheological behavior can be tuned, and how they can be formed into scaffolds using both compression and injection molding processes. In both processes, an aqueous HA-SF paste was molded and subsequently heated to initiate β-sheet crystallization of the silk fibroin to stabilize the structure of the composite. The injection molding of HA-SF composites demonstrated here exhibits similarities to aqueous injection molding, which involves injecting an aqueous thermo-gelling polymer, such as agar, into a mold maintained at a temperature below the sol-gel transition to induce polymer gelation, followed by drying and sintering [34]. However, silk fibroin does not exhibit a sol-gel transition. There are also similarities to powder injection molding (PIM) in which heavily filled polymer system is injection molded to form parts that are subsequently de-bound and sintered. Although extensive research has been done on PIM for HA composites to create bone scaffolds, these composites have never contained silk fibroin [35,36].

2. Materials and methods

Silkworm cocoons from *Bombyx mori* were obtained from Tajima Shoji Co., LTD (Yokohama, Japan. Commercially available hydroxyapatite ($Ca_{10}(PO_4)_6(OH)_2$) was obtained from Fisher Scientific (Pittsburg, PA). All other chemicals and reagents were obtained from Sigma (St. Louis, MO).

2.1. Preparation of regenerated silk fibroin

Bombyx mori silk fibroin solution was prepared as previously described [37]. Briefly, 5 g of silk cocoons were boiled in 2 L of an aqueous solution of 0.02 M sodium carbonate for either 30 or 60 minutes, rinsed with deionized water, and dried. The dry silk fibers were dissolved in a 9.3 M lithium bromide solution (25% wt/v) at 60 °C for 4–6 hours, and the resulting solution was dialyzed against deionized water using 3500 Da molecular weight cut off dialysis tubing (Spectrum Laboratories, Rancho Dominguez, CA) to remove the lithium bromide. The solution was further processed to form soluble silk powder by freezing 8% wt/v aqueous silk solution from either 30-mb or 60-mb (minutes boiled) silk fibroin for 24 hours at −20 °C, and lyophilizing (Labconco, Kansas City, MO) at a pressure of 0.020 Torr for 24–48 hours. After lyophilization, the resulting lyophilized silk was ground into a fine powder using a conventional kitchen blender and stored at low humidity conditions (<30%) until further use.

2.2. Particle size, morphology, and composition

Mean particle size and particle size distribution of hydroxyapatite and silk fibroin powders were determined using dynamic light-scattering particle size analysis (Horiba LA-300, Horiba Instruments Inc., New York, USA). Pre-measured samples of either HA or SF powders (n = 3) were dispersed in 70% isopropanol and sonicated for 2 minutes at 15% amplitude (Misonix Sonicator S-4000, Qsonica Inc., Newtown, CT) prior to particle analysis to break up powder aggregates. Grain size and morphology of the HA or silk fibroin powders was visualized using a field emission scanning electron microscope (FESEM Ultra55, Carl Zeiss AG, Oberkochen, Germany). Dry power samples (n = 3) were sputter coated (SC7620 mini sputter coater, Quorum Technologies, Kent, UK) with gold (5–10 nm) and imaged at a voltage of 5 kV. Phase composition of hydroxyapatite and silk fibroin powder samples (n = 2) was analyzed using a Scintag PAD X powder x-ray diffractometer with a Peltier cooled Si(Li) solid state detector with a 0.5 mm scatter slit and a 0.2 mm receiving slit. A CuKα x-ray source (wavelength 1.54 Å) was operated at a voltage of 45 kV and a current of 40 mA. Samples were scanned at a rate of two degrees per minute.

2.3. Rheological characterization of HA-SF composites

Rheological tests on the HA-SF composite slurries were conducted using an ARES Rheometer (TA Instruments Inc., New Castle, DE) with cone and plate geometry (ø = 25 mm, cone angle = 0.1 rad). For each test, 2 g of HA-SF composite powders containing variable amounts of SF powder (0, 1, 10, or 20% wt/v) was mixed with different amounts of deionized water to achieve the desired powder-to-liquid (P/L) ratio (0.5, 0.6, or 0.7) and mixed for 1 minute to form a slurry. The slurry was then transferred to the cone and plate fixture, and excess slurry was removed from the edges of the cone to ensure full contact of the complete surface area of the cone geometry during testing. Tests were initiated immediately after mixing, and the measurement temperature for all tests was kept constant at 25 °C. The maximum test duration was 2 minutes to minimize drying effects. Steady state testing was conducted over a shear rate ramp from 1 to 100 s^{-1} with a 5 second equilibration time and 5 second measurement time. Each steady rate test was performed independently using a freshly mixed 2-g sample of the HA-SF slurry (n = 3 for each group). To assess the dynamic rheological properties of the HA-SF composites, strain-sweep testing was conducted from 0.1% to 100% strain at a frequency of 1 Hz to determine the linear viscoelastic range of the material. A subsequent frequency sweep was performed at a critical strain of 0.1% over a frequency range of 0.1–100 rad/s. Each frequency-sweep test was conducted independently using a freshly mixed 2-g sample of the HA-SF composite (n = 3 for each group). A no silk fibroin control (0 wt% SF) was tested at each P/L ratio (n = 3) for each of the above tests.

2.4. Compression molding of HA-SF composites

Compression molding of HA-SF composites was performed at room temperature (20-25 °C) using a 120 kN (12 ton) hydraulic press (Carver Inc., Wabash, IN). Molds with varying cavity sizes were used for molding scaffolds (25 mm diameter x 12.75 mm thickness for the largest cavity, 9 mm diameter x 6.25 mm thickness for the smallest cavity). The mold was lined with aluminum foil that was pre-treated with commercial silicone mold release (Smooth-On Inc., Macungie, PA). HA-SF slurries containing 1, 10, or 20 wt% silk fibroin by mass were mixed with water (1.4 mL/g) to obtain a homogenous paste at a P/L ratio of 0.7, and packed into the mold allowing excess material and water to flash through the parting line of the mold. The molds were pressed at 50 kN and held at maximum load for 3 minutes. After pressing, the molds were treated at 60 °C for 48–72 hours to promote complete scaffold drying. The finished scaffolds were removed and stored at ambient conditions until further testing.

2.5. Injection molding of HA-SF composites

Injection molding of the HA-SF composites was carried out using a vertical piston injection molding machine (DACA Instruments Inc., defunct) with a maximum shot size of 7.2 cm^3 (0.24 oz.). An aluminum mold with an edge-gated disk cavity (32 mm diameter by 3 mm thick cavity, 3 mm × 4 mm parabolic runner) was used for the injection molding trials. As with compression molding, the injection mold was lined with aluminum foil and treated with silicone mold release. The barrel temperature was set to the threshold temperature of 30 °C to prevent premature crystallization of the silk fibroin prior to injection. Conversely, the mold temperature was set to 60 °C to initiate silk stabilization and scaffold drying immediately after injection. Batches of HA-SF composites (4 cm^3 total material) containing 1 to 20 wt% silk by mass were mixed with water (1.4 mL/g) to obtain a homogenous paste at a P/L ratio of 0.7, which was loaded into the barrel. Additional clamping tonnage was applied to the mold using screw jacks to prevent flashing and leakage at the nozzle due to the low viscosity of the material compared to conventional thermoplastics. The HA-SF composites were injected at a pressure of 157 bar and were set under packing pressure for 5 minutes at 60 °C. The mold was removed and placed in a 60 °C oven for 48–72 hours to complete the drying of the HA-SF scaffolds. The finished scaffolds were removed and stored at ambient conditions until further testing.

2.6. Scaffold morphology

Structural morphology of the HA-SF scaffolds (n = 3) were visualized using field emission scanning electron microscope (FESEM, Ultra55 or Supra55VP, Carl Zeiss AG, Oberkochen, Germany). Dry samples (5 mm height x 5 mm diameter) were fractured and the inner surfaces of the scaffolds were sputter coated with gold (5–10 nm) and imaged at a voltage of 5 kV.

2.7. Mechanical testing

Compression tests were performed on an Instron E10000 (Instron, Inc., Norwood, MA, USA) testing frame equipped with a 10 kN load cell. The dry HA-SF scaffolds (roughly 23.6 mm diameter x 3.6 mm thickness after drying) were not pre-conditioned prior to testing. Tests were conducted on compression molded samples at a crosshead speed of 2 mm/min and load was applied until a strain of 10% was reached or until fracture occurred. The compressive modulus was calculated as the slope of the linear region of the stress-strain curve. Yield was taken as the inflection point of the elastic region before the plateau on the stress-strain curve. The geometry of the samples was dictated by the compression molds available and it is acknowledged that it does not comply with ASTM standards for ceramics in that the sample diameter is significantly larger than the height. Therefore, the results should be used for comparison purposes.

2.8. Statistical analysis

Statistical analyses were performed with either one-way or two-way analysis of variance (ANOVA) with Bonferroni procedure for post-hoc comparison using GraphPad Prism. $P < 0.05$ was considered statistically significant and significance levels were indicated in each of the figures as $*p < 0.05$, $**p < 0.01$, and $***p < 0.001$.

3. Results

3.1. Hydroxyapatite and silk fibroin characterization

Silk from *B. mori* silkworm cocoons was processed into a soluble silk powder that could be combined with hydroxyapatite to create ceramic-silk fibroin slurries for rheological testing and molding (Fig. 1A). Scanning electron micrographs of the SF and HA precursor materials are shown in Fig. 1B. Particle size distribution analysis (Fig. 1C) revealed that HA particles (10.36 ± 10.26 μm) were significantly smaller than both 30-mb and 60-mb silk particles (247.67 ± 134.81 μm, 230.56 ± 129.18 μm, respectively) (Table 1). Boiling time (degumming time) of the raw silk fibers during processing, which is a critical step for biocompatibility to remove inflammatory sericin protein coating the silk fibers, did not influence the average particle size made by grinding the lyophilized silk fibroin solution. X-ray diffraction spectra showed several major characteristic HA peaks (peaks (002) at 25.9°, (300) at 32.9°, (310) at 39.8°, and (213) at 49.5°) (JCPDS 09–0432), however, no distinct peaks could be identified in the SF powder. The combination of the two showed a hybrid spectrum (Supplemental Figure 1).

3.2. Rheological behavior of HA-SF composites

Rheological testing was conducted to assess the effects of solids loading content (powder-to-liquid ratio), silk fibroin content, and silk fibroin boil time on the flow properties of the HA-SF slurries. The degumming process, which involves boiling the raw silk fibers, strongly influences the molecular weight of the regenerated silk fibroin solution, and the effects of degumming boil time on silk fibroin properties have been thoroughly characterized elsewhere [38]. Under steady-state shear testing, pseudoplastic behavior was observed for all HA-SF composites regardless of powder-to-liquid (P/L) ratio, SF content, or SF boil time. Shear thinning behavior can be seen in representative flow curves shown in Fig. 2A. Powder-to-liquid ratio produced the most dramatic effects on slurry behavior, with slight modifications leading to significant changes in viscosity with increasing shear rate. At a given P/L ratio, however, slurries containing higher SF content reached a constant steady-state viscosity at lower shear rates regardless of SF boil time (Fig. 2B). These differences can be more easily appreciated by comparing slurry viscosity at a specific shear rate of 39 s^{-1} as is done in Fig. 3. For samples made with 10 wt% 60-mb silk fibroin, a change in P/L ratio from 0.5 to 0.6 resulted in a 3.7-fold increase in viscosity, and a further increase by 3.2-fold was observed at a P/L ratio of 0.7 (Fig. 3A). Adjusting SF content also afforded control over slurry viscosity for both 30-mb and 60-mb silk, however, slurries containing 30-mb fibroin exhibited more complex behavior with regards to SF content. A significant drop in viscosity of 30-mb samples did not occur until the SF content reached 20 wt% regardless of P/L ratio. This is evidenced by the fact that only 20 wt% SF slurries made with 30-mb SF exhibited significantly lower viscosities than the 0 wt% SF control ($p < 0.001$ for 20 wt% 30-mb slurries at P/L ratio 0.7), whereas with 60-mb SF both 10 and 20 wt% slurries exhibited significantly lower viscosities than the no SF control ($p < 0.01$ and $p < 0.001$ for 10 wt% and 20 wt% respectively at P/L ratio 0.7) (Fig. 3A). SF boil time also led to significant differences in viscosity with lower boil time corresponding to higher viscosities regardless of P/L ratio or SF

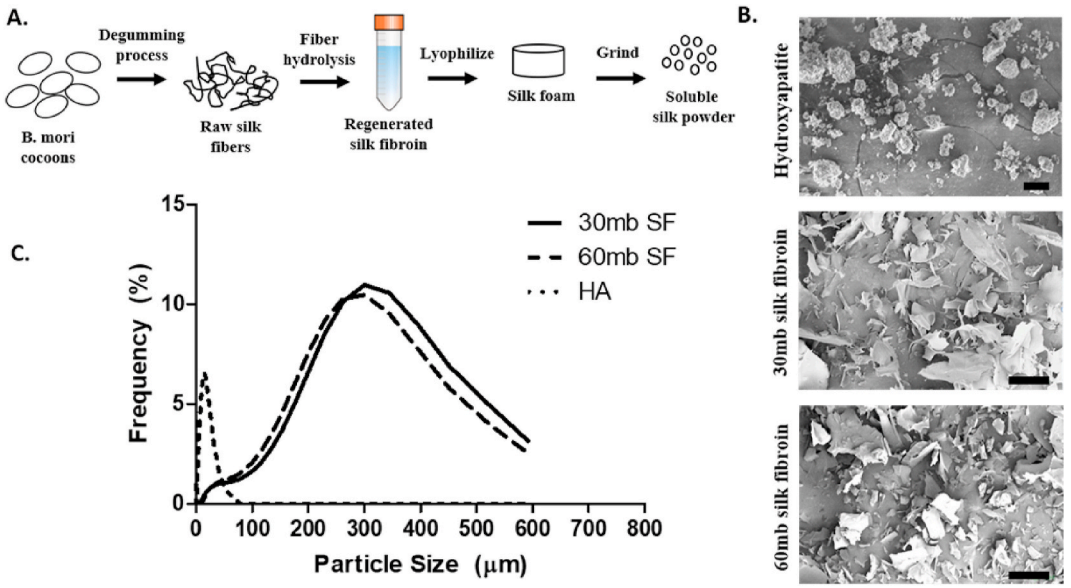

Fig. 1. HA-SF processing and characterization. A. Processing of raw silk fibers from *B. mori* cocoons via degumming and fiber hydrolysis to produce aqueous regenerated silk fibroin (SF) solution which is later lyophilized and ground into powder. B. Scanning electron microscopy images of hydroxyapatite (HA) and SF powders (processed with either 30 min or 60 min of boiling during degumming). Scale bars are 10 μm in the HA image and 200 μm in the SF images. C. Particle size distribution of HA and SF powders.

Table 1
Characterization of HA and SF powders. Mean particle size and specific surface area (n = 3).

Material	Mean particle size (μm)	Std.Dev. (μm)	SSA (m^3)	Std.Dev. (m^3)
Hydroxyapatite	10.36	10.26	56.26	5.51
30-mb SF	247.67	134.81	–	–
60-mb SF	230.56	129.18	–	–

content. However, differences between 30- and 60-mb were generally more pronounced at lower P/L ratio and higher SF content (Fig. 3B).

Frequency sweeps on HA-SF slurries were performed at 1 Hz (6.283 rad/s) in the linear viscoelastic region (0.1% strain) as determined with strain sweep testing (Supplemental Figure 2). Representative frequency sweeps are shown in Fig. 4A for 60-mb silk at a P/L ratio of 0.7. All slurries exhibited dominant storage modulus (*G'*) over loss modulus (*G''*) across the entire range of frequencies tested, with a modest increase in storage modulus with increasing frequency. Effects of SF content and boil time are seen for representative curves at P/L 0.6 in Fig. 4B. Higher SF content significantly decreased the modulus of HA-SF slurries, with a more pronounced effect observed at higher P/L ratios, specifically P/L 0.7 (Fig. 4C). This decrease in modulus was observed for both 30- and 60-mb silk fibroin, however, 60-mb slurries exhibited significantly lower moduli than 30-mb slurries (e.g. 15-fold lower for 1 wt% SF content at P/L ratio 0.7). Slurries containing 30-mb silk fibroin generally displayed a greater dependence on both the SF content and P/L ratio of the samples. This was most evident at a P/L ratio of 0.7 where 30-mb slurries exhibited average storage moduli of 602 kPa, 124 kPa, and 4.6 kPa for SF contents of 1, 10, and 20 wt% respectively. As expected, increasing P/L ratio led to higher dynamic moduli. However, this effect diminished with increasing SF content until samples with 20 wt% silk exhibited moduli that were effectively independent of P/L ratio (Fig. 4D).

3.3. Compression and injection molding of HA-SF composites

Compression molding under standard pressures produced stable composite scaffolds for all HA-SF compositions (Fig. 5A). Stability of the

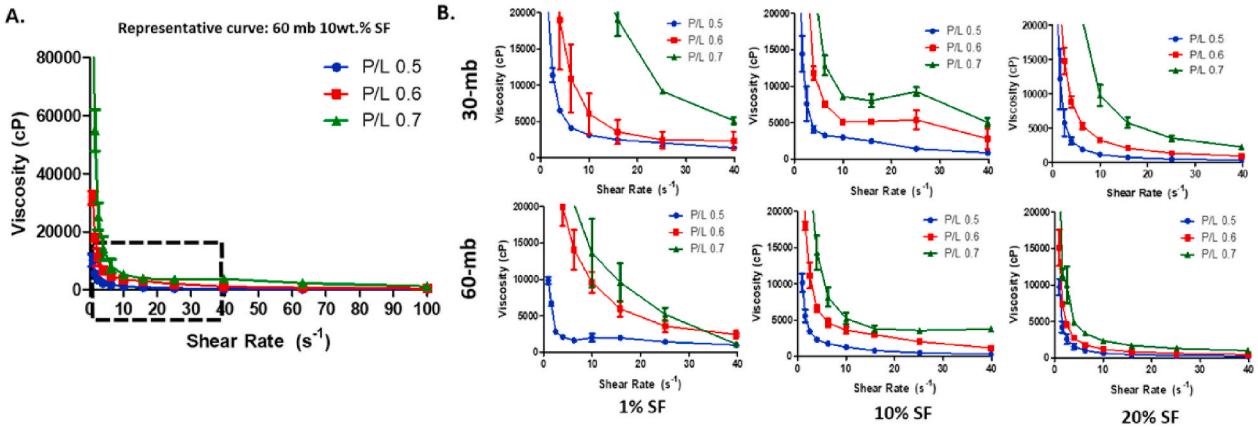

Fig. 2. Shear behavior of HA-SF slurries. A. Representative curve showing shear thinning behavior at all three P/L ratios of HA-SF slurries made with 10 wt% 60-mb SF. B. Magnification of the low shear rate regime (boxed region: 0 to 40 s^{-1}) of shear thinning curves for 30- and 60-min boil SF with varying P/L ratios (0.5, 0.6, and 0.7 ratio of HA:SF) and 1, 10, and 20 wt% SF content (n = 3, error bars are SD).

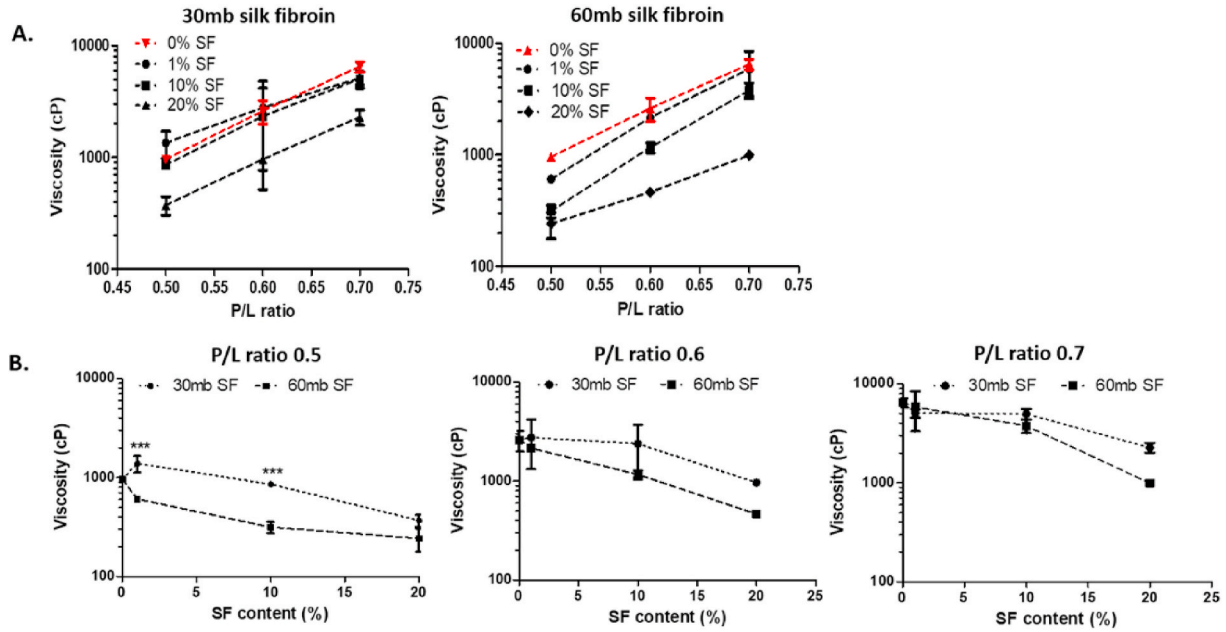

Fig. 3. Effects of SF content, SF molecular weight, and P/L ratio on HA-SF slurry viscosity. A. Influence of powder-to-liquid (P/L) ratio on the viscosity of HA-SF slurries at two different SF molecular weights (as a result of varying silk fibroin degumming time). B. Influence of SF content on HA-SF slurry viscosity shown at three different P/L ratios. Statistical analysis performed with two-way ANOVA with Bonferroni posttest (***$p < 0.001$, $n = 3$, error bars are SD).

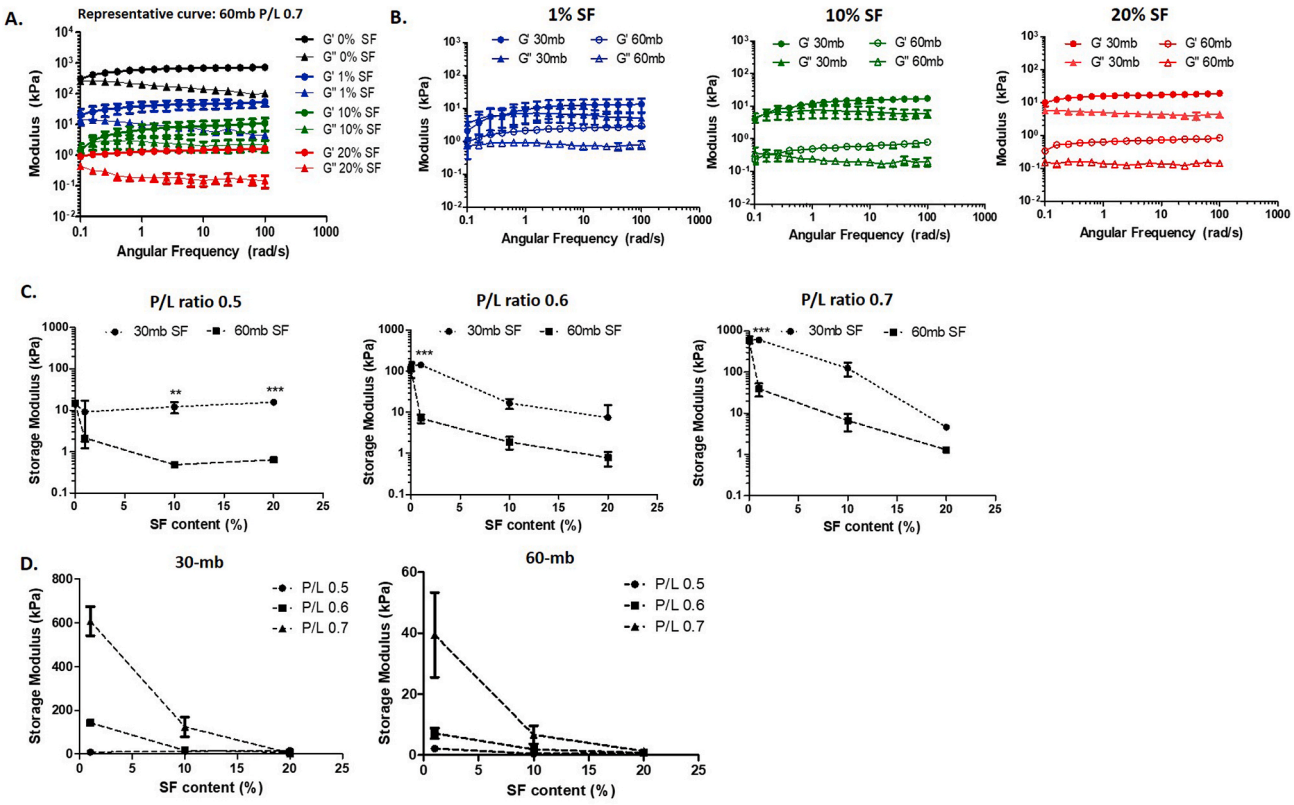

Fig. 4. Dynamic rheological behavior of HA-SF slurries. A. Representative curves from frequency sweep testing (0.1–100 rad/s) on HA-SF slurries performed at 0.1% strain showing differences in G' and G'' as a result of SF content. B. Differences in dynamic rheological behavior of HA-SF slurries as a result of SF content and molecular weight. C. Effects of SF content on storage modulus of HA-SF slurries. D. Effects of P/L ratio on the storage modulus of HA-SF slurries. Statistical analysis performed with two-way ANOVA with Bonferroni posttest (**$p < 0.01$, ***$p < 0.001$, $n = 3$, error bars are SD).

parts increased with higher SF content as observed by flaking of the samples containing low SF content. However, more undesirable adhesion of the HA-SF material to the molding plates was observed at higher SF content. Injection molding trials also successfully produced parts from the investigated HA-SF compositions with more complex geometry (Supplemental Figure 3). However, the geometry of the injection

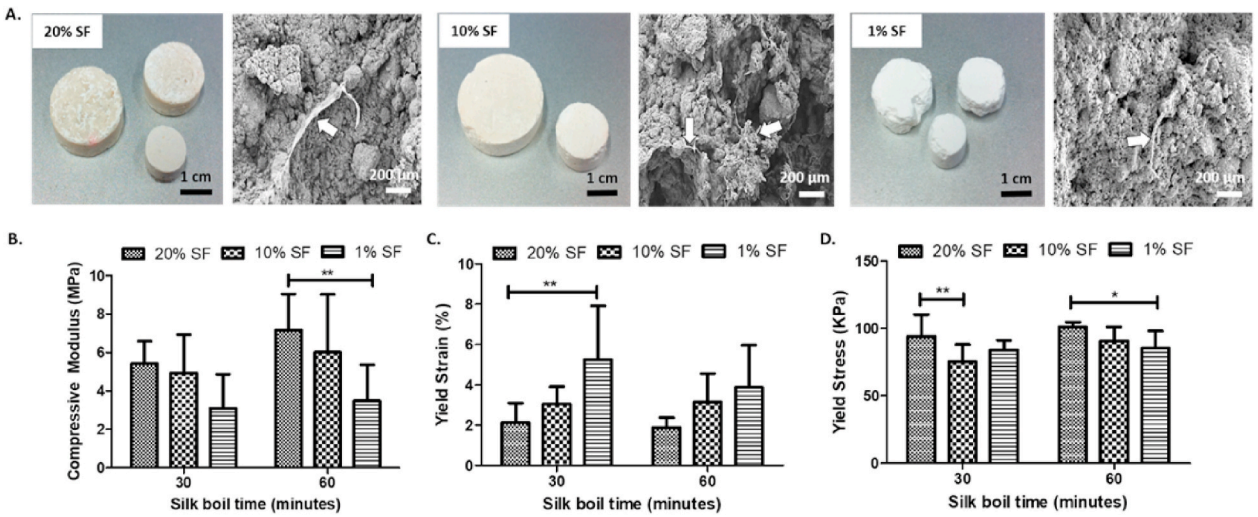

Fig. 5. HA-SF composite scaffold characterization. A. Images of compression molded HA-SF scaffolds with 20, 10, and 1 wt% SF content made with 60-mb SF at a P/L ratio of 0.7 along with corresponding scanning electron microscopy images of fractured surfaces (arrows indicate SF sheets interwoven within the ceramic matrix). Mechanical testing was performed to evaluate the compressive modulus (B), yield strain (C), and yield stress (D) of the HA-SF scaffolds. Statistical analysis performed with two-way ANOVA with Bonferroni posttest (*$p < 0.05$, **$p < 0.01$, $n = 6$, error bars are SD).

molded samples was dictated by the injection molding cavities available and, due to the thin geometry of the cavity, parts made with 1 wt% SF often experienced brittle fracture. As such, mechanical testing was only conducted on compression molded parts. As with compression molding, higher SF content facilitated better scaffold stability after injecting. However, the 20 wt% silk fibroin injection molded samples displayed significant anisotropic shrinkage. Shrinkage in the direction of flow was substantially lower (7.9%) than the transverse direction (11.9%). This is likely due to the pressure gradient across the cavity resulting in lower shrinkage near the gate location.

3.4. HA-SF scaffold characterization

Scanning electron microscopy images of the fractured surfaces of injection and compression molded scaffolds show a composite material of distinct HA and SF components. Strands or sheet-like silk structures can be seen adhering to the ceramic component. (Fig. 5A). SF content in the HA-SF slurries favorably impacted the mechanical strength of the final molded scaffolds. When SF content decreased from 20 wt% to 10 wt % the average compressive modulus of the scaffolds dropped by 9–16%, and the yield stress dropped by 10–20% (Fig. 5A,C). The modulus decreased by another 37–42% when reducing SF content from 10 wt% to 1 wt% silk. There was a noticeable change in mechanical behavior between scaffolds made with 60-mb silk and 30-mb silk. The average compressive modulus of the 60-mb silk scaffolds was 10-24% higher than those made with 30-mb silk, and yield strength was 1–17% higher. SF 60-mb scaffolds containing 20 wt% SF exhibited the highest average compressive modulus of all tested conditions (7.2 ± 1.7 MPa), and those made with 1 wt% 30-mb SF had the lowest compressive modulus (3.1 ± 1.6 MPa) and highest yield strain (Fig. 5A and B).

4. Discussion

Ceramic-biopolymer composites are an attractive option for orthopedic grafting and bone fixation due to their high compressive strength and bioactive properties. The incorporation of silk fibroin with hydroxyapatite has been shown to enhance scaffolds mechanics and serves as an attachment site for cell ingrowth and a depot for drug delivery [39–43]. Due to its highly adhesive, hydrophobic nature, silk protein uniquely enables the fabrication of complex geometry ceramic scaffolds due to its ability to act as a binding agent [30]. However, for ceramic-biopolymer composites to advance towards clinical use, they must be amenable to standard manufacturing production methods. In this study, we showed that injection and compression molding can be used to fabricate reproducible HA-SF composite scaffolds using an aqueous-based formulation. Rheological evaluation performed on HA-SF slurries revealed that slurry viscosity and viscoelastic behavior was strongly influenced by factors such as SF content, SF molecular weight, and powder-to-liquid ratio. HA-SF slurries containing up to 20 wt% silk content were amenable to flow-based injection and compression molding processes, which yielded stable green bodies with mechanical properties that are highly dependent on SF content and molecular weight.

The replacement of thermoplastic carriers that are traditionally used in ceramic molding with a biomaterial to create implants and grafts is highly attractive, however, unless the biopolymer can withstand the harsh processing conditions involved in injection molding it will be unlikely to survive the process without undergoing substantial degradation. The polymer must also afford some control over the flow behavior of the melts and the setting time of the molded parts. Silk is a hydrophobic polymer that exhibits exceptional protein stability to suit this need [44]. A dry SF powder formulation was chosen to generate HA-SF slurries based on the ability of the powder to dissolve rapidly in water forming a dispersant for the HA particles to generate a colloidal suspension. By combining HA with SF in a solid powder form rather than as a solution, the P/L ratio of the slurry could be easily controlled.

Rheological characterization revealed that all HA-SF slurries, regardless of SF content, SF molecular weight, or P/L ratio exhibited shear thinning behavior characteristic of a low solids-loading ceramic suspension. Slurry viscosity and dynamic modulus were significantly impacted by all three parameters. Strain sweep testing showed a small plateau region with yield point at approximately 0.15–0.2% strain. For all slurries, no crossover point was observed in frequency sweep testing and the slurries predominately displayed solid or gel-like properties within the tested frequency range. As expected, P/L ratio, which most significantly impacts the solids loading content of a ceramic slurry, produced a dramatic change in both viscosity and modulus. A narrow range of P/L ratio (0.5–0.7) was selected based on observed differences in rheological behavior and because slurries were not capable of flow above a P/L ratio of 0.7 due to HA particle aggregation. However, although modulating P/L ratio produced large variations in flow behavior, controlling P/L ratio is not ideal for molding ceramic scaffolds since higher water content is inversely related to solids loading and thus sacrifices the strength of the final scaffold.

The combination of SF with HA offers an alternative means of modulating flow behavior since additional parameters such as molecular weight of the silk fibroin can be controlled during silk processing. Longer silk degumming times result in lower molecular weight proteins, with 60 minutes and 30 minutes of extraction producing proteins of approximately 50 kDa and 150 kDa, respectively [45]. Silk fibroin boiled for 60 minutes has a viscosity of 1.6 mPa-s, which is slightly higher than that of water [46]. As expected, slurries made with 60-mb silk consistently displayed lower viscosities and dynamic moduli than those made with 30-mb silk. Increasing the SF molecular weight within the silk dispersant phase of the HA-SF colloidal suspension led to more complex rheological behavior as seen with 30-mb slurries, which did not display a significant drop in viscosity until the silk content reached 20 wt %. A two-fold higher 30-mb silk content (20 wt%) was required to achieve similar viscosity values to slurries made with only 10 wt% 60-mb SF. This suggests that the high molecular weight silk chains may interact to a greater degree with HA particles even at low SF content thus requiring higher shear stress to disrupt the suspension.

Both injection and compression molding produced stable HA-SF composite scaffolds with silk content from 1 to 20 wt%. Parts containing 20 wt% silk were more stable, easier to handle, and exhibited less cracking. However, above 20 wt% silk, the slurries were highly adhesive which disrupted flow into the molding cavity. Mechanical testing revealed that HA-SF green body mechanics were mainly influenced by SF content, however, 60-mb SF green bodies generally displayed higher strength than those containing 30-mb SF. At the tested P/L ratio of 0.7, green body compressive modulus could be controlled with adjustments in SF content and boil time to achieve a range of 3.1–7.2 MPa, thus allowing for tailoring of final scaffold properties. The structural integrity of these formed green bodies is due to the adhesive nature of the silk fibroin which can allow for immediate use after production without the need for further processing. In the green state, these scaffolds match the mechanical properties of human trabecular bone [47].

Despite the advantages of silk fibroin for injection and compression molding of ceramic-biopolymer scaffolds, there are several obstacles that must be overcome for translation of this process. Silk fibroin displays excellent stability in dehydrated and aqueous states, and silk powders retain their solubility and molecular weight distribution after several months of storage [48]. However, once formulated, HA-SF slurries are mainly susceptible to changes in rheological behavior due to aging and may undergo phase separation upon drying or as a result of protein aggregation or crystallization, particularly at elevated temperatures. Since the SF acts as a binding material for the finished scaffolds, this process requires evaporative drying to solidify the molded parts instead of exploiting the phase transformation of a thermoplastic carrier as is done in traditional ceramic injection molding. This evaporative drying is a slow process that requires longer periods of time than would be used in standard industrial molding equipment. A few process modifications could be envisioned to scale up this process for manufacturing including using molds with specially designed vents to facilitate drying, incorporating low-pressure drying ovens, and using multiple molds on a continuous production line. Additionally, while our study investigates the rheological control of HA-SF composites using non-reactive calcium phosphate and proves the feasibility of molding ceramic with silk fibroin, the practical application of silk in combination with ceramic for injection molding may be better suited with a self-setting calcium phosphate mixed with silk fibroin.

5. Conclusion

Combining natural biopolymers with ceramics has created a field of composite tissue engineering that takes advantage of the unique mechanical and biological properties of both materials to create optimally bioengineered grafts for bone replacement or fracture fixation. However, to be amenable to large-scale manufacturing, the biopolymer must withstand harsh conditions associated with industrial molding techniques that are traditionally used with synthetic thermoplastic materials. Here we demonstrate the feasibility of injection and compression molding of hydroxyapatite combined with natural silk fibroin protein. The robustness of the silk protein enables it to be molded in combination with hydroxyapatite into stable, composite green bodies using standard injection and compression molding methods. The tunable properties of silk fibroin afford control over the rheological behavior and flow characteristics of the HA-SF slurries during molding without compromising the density, strength, and integrity of the molded parts. The unique properties of silk could offer a potential for low cost, reproducible manufacturing of bioactive ceramic-silk grafts and orthopedic implants.

Author contributions statement

S.L.M., S.P.J., and D.L.K. conceived the research design. S.L.M, E.M.M, and D.F.S performed the experiments. S.L.M., E.M.M., and D.F.S conducted data processing. S.L.M, S.P.J., D.F.S., and E.M.M. contributed to analysis and interpretation of data. S.L.M. and E.M.M drafted the manuscript. All authors reviewed and edited the manuscript.

Declaration of competing interest

The authors declare that they have no known competing financial interests or personal relationships that could have appeared to influence the work reported in this paper.

Acknowledgements

The authors thank the NIH (grants P41EB027062 and R01AR068048) for funding support.

Appendix A. Supplementary data

Supplementary data to this article can be found online at https://doi.org/10.1016/j.biomaterials.2020.120643.

References

[1] R.C. Gardner, Complication of excessive compression and rigid internal fixation, J. Trauma 12 (6) (1972) 534–536.
[2] R.R. Bos, G. Boering, F.R. Rozema, J.W. Leenslag, Resorbable poly(L-lactide) plates and screws for the fixation of zygomatic fractures, J. Oral Maxillofac. Surg. 45 (9) (1987) 751–753.
[3] S.A. Tatum, Retrospective review of resorbable plate fixation in pediatric craniofacial surgery long-term outcome, Arch. Facial Plast. Surg. 14 (1) (2012) 11–13.
[4] R. Suuronen, R. Kontio, N. Ashammakhi, C. Lindqvist, P. Laine, Bioabsorbable self-reinforced plates and screws in craniomaxillofacial surgery, Bio Med. Mater. Eng. 14 (4) (2004) 517–524.
[5] O. Bostman, H. Pihlajamaki, Clinical biocompatibility of biodegradable orthopaedic implants for internal fixation: a review, Biomaterials 21 (24) (2000) 2615–2621.
[6] H.P. Yuan, H. Fernandes, P. Habibovic, J. de Boer, A.M.C. Barradas, A. de Ruiter, W.R. Walsh, C.A. van Blitterswijk, J.D. de Bruijn, Osteoinductive ceramics as a synthetic alternative to autologous bone grafting, Proc. Natl. Acad. Sci. Unit. States Am. 107 (31) (2010) 13614–13619.
[7] M. Bohner, Calcium orthophosphates in medicine: from ceramics to calcium phosphate cements, Injury 31 (2000). S-D37-D47.
[8] N. Doebelin, R. Luginbuehl, M. Bohner, Synthetic calcium phosphate ceramics for treatment of bone fractures, Chimia 64 (10) (2010) 723–729.
[9] W. Swieszkowski, Z. Jaegermann, D.W. Hutmacher, K.J. Kurzydlowski, Ceramic materials for bone tissue replacement and regeneration, in: D.L. Jiang, Y.P. Zeng, M. Singh, J. Heinrich (Eds.), Ceram Trans, 2010, pp. 525–530.
[10] S. Esmaeili, H.A. Aghdam, M. Motififard, S. Saber-Samandari, A.H. Montazeran, M. Bigonah, E. Sheikhbahaei, A. Khandan, A porous polymeric–hydroxyapatite scaffold used for femur fractures treatment: fabrication, analysis, and simulation, Eur. J. Orthop. Surg. Traumatol. 30 (1) (2020) 123–131.
[11] C.E. Corcione, F. Gervaso, F. Scalera, S.K. Padmanabhan, M. Madaghiele, F. Montagna, A. Sannino, A. Licciulli, A. Maffezzoli, Highly loaded hydroxyapatite microsphere/PLA porous scaffolds obtained by fused deposition modelling, Ceram. Int. 45 (2) (2019) 2803–2810.

[12] S. Mondal, T.P. Nguyen, G. Hoang, P. Manivasagan, M.H. Kim, S.Y. Nam, J. Oh, Hydroxyapatite nano bioceramics optimized 3D printed poly lactic acid scaffold for bone tissue engineering application, Ceram. Int. 46 (3) (2020) 3443–3455.
[13] J.O. Akindoyo, M.D. Beg, S. Ghazali, H.P. Heim, M. Feldmann, Effects of surface modification on dispersion, mechanical, thermal and dynamic mechanical properties of injection molded PLA-hydroxyapatite composites, Composer Part A - Applied 103 (2017) 96–105.
[14] F. Witte, T. Calliess, H. Windhagen, Biodegradable synthetic implant materials. Clinical applications and immunological aspects, Orthopade 37 (2) (2008) 125–130.
[15] Y.H. An, S.K. Woolf, R.J. Friedman, Pre-clinical in vivo evaluation of orthopaedic bioabsorbable devices, Biomaterials 21 (24) (2000) 2635–2652.
[16] P. Saini, M. Arora, M. Kumar, Poly(lactic acid) blends in biomedical applications, Adv. Drug Deliv. Rev. 107 (2016) 47–59.
[17] M. Murariu, P. Dubois, PLA composites: from production to properties, Adv. Drug Deliv. Rev. 107 (2016) 17–46.
[18] S.V. Dorozhkin, Calcium orthophosphate cements and concretes, Materials 2 (1) (2009) 221–291.
[19] S.V. Dorozhkin, Bioceramics of calcium orthophosphates, Biomaterials 31 (7) (2010) 1465–1485.
[20] S.V. Dorozhkin, Calcium orthophosphate-based biocomposites and hybrid biomaterials, J. Mater. Sci. 44 (9) (2009) 2343–2387.
[21] D. Wahl, J. Czernuszka, Collagen-hydroxyapatite composites for hard tissue repair, Eur. Cell. Mater. 28 (11) (2006) 43–56.
[22] S. Kobayashi, K. Sakamoto, Bending and compressive properties of crystallized TCP/PLLA composites, Adv. Compos. Mater. 18 (3) (2009) 287–295.
[23] R.A. Mickiewicz, A.M. Mayes, D. Knaack, Polymer-calcium phosphate cement composites for bone substitutes, J. Biomed. Mater. Res. 61 (4) (2001) 581–592.
[24] S.J. Stedman, J.R.G. Evans, R.J. Brook, M.J. Hoffmann, Anisotropic sintering shrinkage in injection molded composite ceramics, J. Eur. Ceram. Soc. 11 (6) (1993) 523–532.
[25] R.H. Chen, C.H. Ho, H.C. Fan, Shrinkage properties of ceramic injection moulding part with a step-contracted cross-section in the filling direction, Ceram. Int. 30 (6) (2004) 991–996.
[26] M.J. Edirisinghe, Fabrication of engineering ceramics by injection molding, Am. Ceram. Soc. Bull. 70 (5) (1991) 824–828.
[27] R.M. German, K.F. Hens, S.T.P. Lin, Key issues in powder injection molding, Am. Ceram. Soc. Bull. 70 (8) (1991) 1294–1302.
[28] E. Medvedovski, M. Peltsman, Low pressure injection moulding mass production technology of complex shape advanced ceramic components, Adv Appl Ceram 111 (5–6) (2012) 333–344.
[29] J.C. Middleton, A.J. Tipton, Synthetic biodegradable polymers as orthopedic devices, Biomaterials 21 (23) (2000) 2335–2346.
[30] S.L. McNamara, J. Rnjak-Kovacina, D.F. Schmidt, T.J. Lo, D.L. Kaplan, Silk as a biocohesive sacrificial binder in the fabrication of hydroxyapatite load bearing scaffolds, Biomaterials 35 (25) (2014) 6941–6953.
[31] L. Meinel, R. Fajardo, S. Hofmann, R. Langer, J. Chen, B. Snyder, G. Vunjak-Novakovic, D. Kaplan, Silk implants for the healing of critical size bone defects, Bone 37 (5) (2005) 688–698.
[32] Y. Gu, L. Chen, H.L. Yang, Z.P. Luo, T.S. Tang, Evaluation of an injectable silk fibroin enhanced calcium phosphate cement loaded with human recombinant bone morphogenetic protein-2 in ovine lumbar interbody fusion, J. Biomed. Mater. Res. 97A (2) (2011) 177–185.
[33] C. Cao, H. Li, J. Li, C. Liu, H. Yang, B. Li, Mechanical reinforcement of injectable calcium phosphate cement/silk fibroin (SF) composite by mineralized SF, Ceram. Int. 40 (9) (2014) 13987–13993.
[34] I. Santacruz, M.I. Nieto, R. Moreno, P. Ferrandino, A. Salomoni, I. Stamenkovic, Aqueous injection moulding of porcelains, J. Eur. Ceram. Soc. 23 (12) (2003) 2053–2060.
[35] A. Arifin, A.B. Sulong, N. Muhamad, J. Syarif, M.I. Ramli, Material processing of hydroxyapatite and titanium alloy (HA/Ti) composite as implant materials using powder metallurgy: a review, Mater. Des. 55 (2014) 165–175.
[36] J. Biggemann, P. Hoffmann, I. Hristov, S. Simon, P. Müller, T. Fey, Injection molding of 3-3 hydroxyapatite composites, Materials 13 (8) (2020) 1907.
[37] D.N. Rockwood, R.C. Preda, T. Yucel, X. Wang, M.L. Lovett, D.L. Kaplan, Materials fabrication from Bombyx mori silk fibroin, Nat. Protoc. 6 (10) (2011) 1612–1631.
[38] L.S. Wray, X. Hu, J. Gallego, I. Georgakoudi, F.G. Omenetto, D. Schmidt, D. L. Kaplan, Effect of processing on silk-based biomaterials: reproducibility and biocompatibility, J. Biomed. Mater. Res. B Appl. Biomater. 99B (1) (2011) 89–101.
[39] M.F. Gan, H.L. Yang, Y.Z. Gu, X.Q. Chen, G.L. Wang, L. Chen, X.S. Zhu, R.J. Xie, Effect of silk fibroin on cell compatibility of injectable calcium phosphate cement, J. Clin. Rehabilitative Tissue Eng. Res. 13 (3) (2009) 427–431.
[40] T. Diab, E.M. Pritchard, B.A. Uhrig, J.D. Boerckel, D.L. Kaplan, R.E. Guldberg, A silk hydrogel-based delivery system of bone morphogenetic protein for the treatment of large bone defects, J Mech Behav Biomed Mater 11 (2012) 123–131.
[41] P. He, S. Sahoo, K.S. Ng, K. Chen, S.L. Toh, J.C. Goh, Enhanced osteoinductivity and osteoconductivity through hydroxyapatite coating of silk-based tissue-engineered ligament scaffold, J. Biomed. Mater. Res. 101 (2) (2013) 555–566.
[42] J. Kundu, Y.-I. Chung, Y.H. Kim, G. Taeb, S.C. Kundu, Silk fibroin nanoparticles for cellular uptake and control release, Int. J. Pharm. 388 (1–2) (2010) 242–250.
[43] X. Chen, H. Yang, M. Gan, R. Xie, L. Chen, X. Zhu, G. Wang, Y. Gu, Influences of silk fibroin on the compressive strength and injectability of calcium phosphate cement, J. Clin. Rehabilitative Tissue Eng. Res. 12 (45) (2008) 8985–8988.
[44] J.M. Gosline, M.E. DeMont, M.W. Denny, The structure and properties of silk, Endeavor 10 (1) (1986) 37–43.
[45] L.S. Wray, J. Rnjak-Kovacina, B.B. Mandal, D.F. Schmidt, E.S. Gil, D.L. Kaplan, A silk-based scaffold platform with tunable architecture for engineering critically-sized tissue constructs, Biomaterials 33 (36) (2012) 9214–9224.
[46] Z. Wang, H. Yang, W. Li, C. Li, Effect of silk degumming on the structure and properties of silk fibroin, J. Text. Inst. 110 (1) (2019) 134–140.
[47] L.J. Gibson, The mechanical behavior of cancellous bone, J. Biomech. 18 (5) (1985) 317–319.
[48] J.A. Kluge, B.T. Kahn, J.E. Brown, F.G. Omenetto, D.L. Kaplan, Optimizing molecular weight of lyophilized silk as a shelf-stable source material, ACS Biomater. Sci. Eng. 2 (4) (2016) 595–605.